



UNIVERSITY OF LEEDS

This is a repository copy of *Late diagenesis of illite-smectite in the Podhale Basin, southern Poland: Chemistry, morphology, and preferred orientation*.

White Rose Research Online URL for this paper:
<http://eprints.whiterose.ac.uk/125140/>

Version: Accepted Version

Article:

Day-Stirrat, RJ, Aplin, AC, Kurtev, KD et al. (3 more authors) (2017) Late diagenesis of illite-smectite in the Podhale Basin, southern Poland: Chemistry, morphology, and preferred orientation. *Geosphere*, 13 (6). pp. 2137-2153. ISSN 1553-040X

<https://doi.org/10.1130/GES01516.1>

(c) 2017, Geological Society of America. This is an author produced version of a paper published in *Geosphere*. Uploaded in accordance with publisher's self-archiving policy.

Reuse

Items deposited in White Rose Research Online are protected by copyright, with all rights reserved unless indicated otherwise. They may be downloaded and/or printed for private study, or other acts as permitted by national copyright laws. The publisher or other rights holders may allow further reproduction and re-use of the full text version. This is indicated by the licence information on the White Rose Research Online record for the item.

Takedown

If you consider content in White Rose Research Online to be in breach of UK law, please notify us by emailing eprints@whiterose.ac.uk including the URL of the record and the reason for the withdrawal request.



eprints@whiterose.ac.uk
<https://eprints.whiterose.ac.uk/>

1 **Late Diagenesis of Illite-Smectite in the Podhale Basin: Chemistry, Morphology and**
2 **Preferred Orientation**

3
4

5 Ruarri J. Day-Stirrat^{1*}, Andrew C. Aplin², Kuncho D. Kurtev³, Anja M. Schleicher⁴, Andrew P.
6 Brown⁵ and Jan Środoń⁶

7

8 ¹ Shell International E&P Inc, Shell Technology Center-Houston, 3333 Highway 6 South,
9 Houston, Tx, 77082, USA

10 ² Department of Earth Sciences, Durham University, Durham, DH1 3LE, U.K.

11 a.c.aplin@durham.ac.uk

12 ³ SINTEF, Sem Sælands vei 11, 7034, Trondheim, Norway. Kuncho.Kurtev@sintef.no

13 ⁴ Helmholtz Centre Potsdam, GFZ German Research Centre for Geosciences, Telegrafenberg,
14 Building B, room 327, 14473 Potsdam, Germany. anja.maria.schleicher@gfz-potsdam.de

15 ⁵ Institute for Materials Research, University of Leeds, Leeds, LS2 9JT, UK.

16 A.P.Brown@leeds.ac.uk

17 ⁶ Institute of Geological Sciences, PAN, Senacka 1, 31-002 Kraków, Poland [ndsrodon@cyf-](mailto:ndsrodon@cyf-kr.edu.pl)
18 [kr.edu.pl](mailto:ndsrodon@cyf-kr.edu.pl)

19 *Corresponding Author:

20 Dr. Ruarri J. Day-Stirrat

21 Shell International E&P Inc, Shell Technology Center-Houston, 3333 Highway 6 South, Houston,
22 Tx, 77082, USA

23 E-mail: ruarri.day-stirrat@shell.com

24

25 **Abstract**

26 Well-characterized samples from the Podhale Basin, southern Poland, formed the basis for
27 exploring and illuminating subtle diagenetic changes to a mudstone towards the upper end of the
28 diagenetic window, prior to metamorphism. Transmission Electron Microscopy (TEM)
29 performed on dispersed grains and ion-beam thinned preparations, Selected Area Diffraction
30 Patterns (SAED) and chemistry by TEM-EDS (Energy Dispersive Spectra) augmented
31 mineralogy and fabric data. The deepest samples show no change in their percent illite in illite-
32 smectite (I-S), yet I-S phase octahedral Fe^{3+} and Al^{3+} are statistically different between samples.
33 A decrease in the in the Fe^{3+} concentration in the octahedral sheet correlates with an increase in
34 I-S fabric intensity and apparent crystallinity. The D-statistic from the Kolmogorov-Smirnov (K-
35 S) test on TEM-EDS data describes statistical differences between the I-S chemistry. Previous
36 work on these samples showed a significant increase in the preferred orientation of the I-S phase
37 across the smectite-to-illite transition and a significant slowdown in the rate of development of
38 preferred orientation beyond the termination of smectite illitization. Lattice fringe images
39 describe an I-S morphology that coalesces into large and tighter packets with increasing burial
40 temperature and a decrease in I-S packet contact angle, yet some evidence for smectite collapse
41 structures is retained. The deepest sample shows the thickest, most coherent I-S packets. We
42 propose that the deepest samples in the Podhale Basin describe the precursor stage in
43 phyllosilicate fabric preferred orientation increase from diagenesis into metamorphism, where
44 continued evolution of crystallite packets and associated crystallinity create higher I-S fabric
45 intensities as the structural formulae of I-S approaches an end-member composition.

46

47 Keywords: Late-diagenesis; Illite-smectite; Micro-Fabric; Shale; Mudstone

48

49

50 **1. Introduction**

51 The physical, chemical and mineralogical changes which transform muds into mudstones
52 and ultimately metamorphic pelites have been studied for many years (Sorby, 1853; Rieke and
53 Chilingarian, 1974; Weaver, 1989; Bjørlykke and Høeg, 1997). With respect to mineralogical
54 change, particular attention has been paid to the major reactions involving clay minerals, most
55 obviously the transformation of smectite to illite and additional mineral changes, for example
56 quartz and chlorite precipitation, associated with that reaction (e.g. Perry and Hower, 1970; Hower
57 et al., 1976; Boles and Franks, 1979; Nadeau et al., 2002). Whilst X-ray diffraction has charted the
58 mineralogical changes, Transmission Electron Microscopy (TEM) has been used to examine the
59 microstructural and chemical changes involved not only in the smectite to illite transformation
60 (Ahn and Peacor, 1986; Bell, 1986; Klimentidis and Mackinnon, 1986; Inoue et al., 1987a; Inoue
61 et al., 1987b; Jiang et al., 1994; Hover et al., 1999; Masuda et al., 2001; Nadeau et al., 2002; Kim
62 et al., 2004), but also in the reactions involved in low grade metamorphism (Merriman and Peacor,
63 1998; Merriman, 2002).

64 Other work has focused on the processes by which the initially random arrangement of
65 phyllosilicate minerals in mud becomes organized into the highly aligned fabric observed in
66 metapelites (Oertel and Curtis, 1972; Curtis et al., 1980; Ho et al., 1999; Jacob et al., 2000; Aplin
67 et al., 2006; Day-Stirrat et al., 2008a; Day-Stirrat et al., 2008b). Discussion has centered on the
68 relative roles of mechanically-driven rearrangement of particles and mineralogical changes in
69 which neoformed phyllosilicate minerals grow normal to the principal effective stress. Whilst
70 laboratory compaction experiments show that mechanical rearrangement of phyllosilicates is
71 feasible (Djéran-Maigre et al., 1998; Haines et al., 2009; Voltolini et al., 2009; Day-Stirrat et al.,
72 2011), both Ho et al. (1999) and Day-Stirrat et al. (2008a) observed a major enhancement to the

73 preferred orientation of I-S across the smectite to illite transition in the Gulf of Mexico and the
74 Podhale Basin of southern Poland, respectively. Day-Stirrat et al. (2008a) suggested that the
75 enhanced fabric intensity through the smectite to illite transition window was indicative of
76 dissolution of smectite and growth of new illite perpendicular to principal effective stress.

77 The changes in phyllosilicate fabric observed at the end of the main smectite to illite
78 transition are nevertheless substantially lower than those observed in low grade metapelites (Jacob
79 et al., 2000). This implies continuing rearrangement of fabric at temperatures and stresses higher
80 than those associated with the smectite illitization. In contact metamorphism, enhancement of
81 phyllosilicates fabrics close to the heating body have been recorded (Ho et al., 1995). In the
82 Podhale Basin (Figure 1), Day-Stirrat et al.'s (2008a) data tentatively suggested a continued
83 increase in I-S (and chlorite) fabric intensity beyond the apparent termination of the smectite to
84 illite transition or certainly the mineral reaction slowdown (Figure 2). This slowdown occurs over
85 an additional burial of 2 km and a temperature increase of 40°C (approximately 115°C to 150°C).
86 Since the porosity of these deeply buried samples is low and pore sizes are smaller than grains,
87 increases in the alignment of phyllosilicate grains are unlikely to result from mechanical processes,
88 but rather from dissolution and reprecipitation processes which may be revealed by changes in I-
89 S chemistry or microfabric. Changes in mineral chemistry have implications for density, and
90 microfabric impacts anisotropy and velocity. The practical importance of these changes is that both
91 density and velocity are key parameters in estimating both porosity and pore pressure in mud-rich
92 sequences, particularly in circumstances where sediments have been unloaded (Bowers, 1995;
93 Lahann and Swarbrick, 2011; Goultly and Sargent, 2016; Goultly et al., 2016). Since relationships
94 between vertical effective stress (VES) and porosity/density are difficult to constrain in
95 diagenetically mature samples (Yang and Aplin, 2004), an examination of the detailed chemistry
96 of mineral change in a low porosity system is timely.

97 In this study, therefore, we take some well-characterized samples from the deepest part of
98 the Podhale Basin and perform transmission electron microscopy (TEM) on both dispersed grains
99 and ion-beam thinned preparations. The TEM-EDS data allow us to look for compositional
100 changes at and beyond the smectite to illite transition, whilst lattice fringe images allow a visual
101 description of the change in crystallite morphology, thickness and fabric. The samples in this paper
102 thus represent a part of the journey a mud takes on its journey to a metamorphic pelite.

103

104 **2. Geological setting and data background**

105 The Palaeogene Podhale Basin of southern Poland is situated between the Pieniny Klippe
106 Belt to the north and the Tatra Mountains to the south (Figure 1). The basin is filled with what is
107 termed the Podhale Flysch (Olszewska and Wieczorek, 1998), deposited by submarine fans
108 (Westwalewicz-Magilska, 1986) and covering a Mesozoic basement that is exhumed in the Tatra
109 Mountains.

110 X-ray diffraction results (Table 1) on the Palaeogene mudstones (Środoń et al., 2006a)
111 describe an extremely homogeneous detrital mineral composition, with regular and clear
112 diagenetic trends with depth. Based on grain-density trends Środoń et al. (2006b) argue that two
113 wells, Chochółów PIG-1 and Bukowina Tatrzańska PIG-1, can be seen as a continuous burial
114 profile, in which a ~500m overlap produces a continuous trend in percentage of smectite in the
115 mixed-layer phase illite-smectite, as well as predictable increases in quartz and chlorite and
116 decreases in kaolinite and potassium feldspar. Present day and calculated palaeo-geothermal
117 gradients are similar in both wells ($\sim 20\text{-}25^\circ\text{C km}^{-1}$). The overlap proposed by Środoń et al (2006b)
118 is consistent with thermal maturity data from Poprawa and Marynowski (2005). The maximum
119 burial of the Podhale Basin was achieved at ~17 Ma, based on K-Ar dates from clay mineral
120 separates from bentonites (Środoń et al., 2006b) and maximum burial was deeper than present day

121 burial. Marynowski et al. (2006) present a burial history profile through the center of the basin that
122 shows rapid Oligocene burial followed by Miocene uplift. Porosity data recorded by Day-Stirrat
123 et al. (2008a) show a consistent decrease through the established synthetic profile. The area was
124 the subject of an apatite fission track analysis by Anczkiewicz (2006), who also concluded that the
125 top of Bukowina Tatrzańska PIG-1 had previously been much deeper (totally reset tracks) than the
126 top of Chochołów PIG-1 (partially reset tracks) and subsequently it was eroded.

127 The smoothness of the diagenetic trends (Środoń et al., 2006b), the continuity of physical
128 trends in grain density (Środoń et al., 2006b), phyllosilicate preferred orientation and porosity
129 (Day-Stirrat et al., 2008a) and rapid burial and uplift (Anczkiewicz, 2006) suggest that the
130 submarine fan depositional system described by Westwalewicz-Magilska (1986) was fed by a
131 consistent source area over the period of deposition. The rapid burial of the fore-arc basin system
132 (Tari et al., 1993) of the Podhale flysch probably mitigated significant progradation of the
133 submarine fans leading to the consistent trends noted above, due to a consistent provenance.

134

135 **3. Samples and Methods**

136 **3.1 Samples**

137 The sample set consists of four fragments of cores selected from two boreholes in the
138 Podhale Basin (Figure 1): Chochołów PIG-1 in the west (samples Chochołów-06 and Chochołów-
139 60) and Bukowina Tatrzańska PIG-1 in the east (Bukowina Tatrzańska-06 and Bukowina
140 Tatrzańska-41). These samples cover a maximum temperature and depth range of ~ 50 - 150 °C
141 and 2500 – 7000 m original depth of burial (Table 1). Additional detailed sample information can
142 be found in Marynowski et al. (2006), Środoń et al. (2006b) and Day-Stirrat et al. (2008a). Sample

143 Chochołów-06 has 50% illite in illite-smectite whereas, Chochołów-60, Bukowina Tatrzańska-06,
144 and Bukowina Tatrzańska-41 all have 76% illite in illite-smectite.

145

146 **3.2 Transmission Electron Microscopy**

147 Chemistry of individual illite-smectite phyllosilicate particles was determined using TEM-
148 EDS; crystallite images and selected area diffraction patterns (SAED) were also obtained. Samples
149 were examined at the University of Leeds using a Philips/FEI CM200 electron microscope
150 equipped with a Field Emission Gun (FEG), and a Gatan Imaging Filter (GIF). The extinction
151 voltage was set at 3.21 kV, giving a typical energy resolution of 0.8 eV.

152 Mudstone samples were disaggregated using a gentle freeze-thaw method which does not
153 crush individual particles (Yang and Aplin, 1997). The less than 2 μ m fraction of the sample was
154 then separated by centrifugation. Selected < 2 μ m fractions were prepared for TEM-EDS by
155 dispersing 0.2 g of sample in excess ethanol. Approximately 10 μ L of the dilute suspension was
156 placed on a carbon coated 200-mesh copper grid and allowed to evaporate to dryness. This
157 technique assumes that phyllosilicate particles are aligned with (001) planes approximately
158 perpendicular to the electron beam (c^* parallel to beam). Care was taken to obtain SAED patterns
159 from thin grains, free from the overlap of other grains. Magnification was at 50,000x and Energy
160 Dispersive Spectra (EDS) data were acquired at between 1000 and 3000 counts per second with a
161 live time of 50 seconds using a 75 \AA beam diameter on the same spot as the SAED. Biotite and
162 paragonite standards were used to obtain K-factors for the transformation of intensity ratios to
163 concentrations (Cliff and Lorimer, 1975). Oxygen was not measured as it is strongly affected by
164 differences in sample thickness. Atomic concentration ratios were converted into normalized
165 mineral formulae using an anionic charge of 22 ($\text{O}_{10}[\text{OH}]_2$) and assuming that all iron occurs as
166 Fe^{3+} (Weaver, 1989; Moore and Reynolds, 1997). Oxide weight percents were calculated by

167 normalizing the atomic ratios to 95 wt% (Merriman et al., 1995). Since alkali loss, particularly
168 potassium, is a significant problem in TEM-EDS analysis (van der Pluijm et al., 1988), a consistent
169 50 second count time was used for all samples. A loss of potassium was assumed and the sodium
170 content was not included in the normalization calculations. Omitting Na^+ from the mineral formula
171 does not seriously affect interlayer charge as it comprises <0.1 cations per unit formula. All Mg^{2+}
172 and Fe^{3+} were assigned to the octahedral sheet. Estimated uncertainties in the atomic proportions
173 are: Si^{4+} and Al^{3+} , $\sim \pm 0.1$ cations per unit formula; Fe^{3+} , Mg^{2+} , Ti^{4+} , $\sim \pm 0.05$ cations per unit
174 formula; K^+ , $\sim \pm 0.2$ cations per unit formula (Peacor, 1992; Warren and Ransom, 1992).

175 A thin-section previously prepared for backscattered electron imaging (Day-Stirrat et al.
176 2008a) produced a sample stub that was cut 200-400 μm for high resolution X-ray texture
177 goniometry (Day-Stirrat et al., 2008a). The same sample stub was prepared for lattice fringe
178 imaging with a L.R. White resin treatment (Kim et al., 1995) and was used prior to sample
179 preparation in order to prevent the collapse of smectite layers in the high vacuum environment of
180 the TEM. The preparation aimed to look at I-S in its a or b planes (c^* perpendicular to beam).
181 TEM in this mode has the ability to image the size of crystallite packets and document layer
182 terminations between crystallites. Three millimeter diameter aluminum washers were attached to
183 randomly selected areas on the prepared TEM thin-section and the sample was ion-beam thinned
184 and carbon coated for TEM observation. Lattice fringe observations were obtained using a Phillips
185 CM12 Scanning Transmission Electron Microscope (STEM) at the University of Michigan. The
186 STEM was operated at an accelerating voltage of 120 kV and a beam current of ~ 10 nA.

187

188 **3.3 Statistical Analysis (Kolmogorov-Smirnov test)**

189 The Kolmogorov-Smirnov test (K-S Test) is a method that expresses the similarity or
190 difference between two datasets (Stuart et al., 1999). The test was used on TEM-EDS data from

191 the Podhale Basin samples. The K-S Test is non-parametric and does not require a particular
192 distribution of data (e.g. data normally distributed). It can be used on small datasets (8-13 results),
193 where simply presenting the arithmetic average of a result implies a normal distribution, and also
194 enables the K-S test a visual appraisal of the similarity of datasets. For a dataset of 20 points, the
195 test is very simple but powerful, the data are ordered and the lowest value plotted at 0.05 (1/20);
196 the second lowest value would be plotted at 0.1 (2/20), and so on up to 1 to complete the cumulative
197 distribution. Distributions can be compared visually, and a D-statistic is calculated as the
198 maximum difference or separation between two cumulative distributions and expressed as a
199 percentage.

200

201 **4. Results**

202 **4.1 Selected Area Diffraction Patterns (SAED)**

203 Morphologies of grains for which selected area diffraction patterns were obtained range
204 from euhedral crystallites (Figure 3) to subhedral crystallites (Figure 4). The associated SAED
205 patterns, taken at thin edges of crystallites, have a strong hexagonal arrangement of single crystal
206 diffraction spots in all samples. These spots correspond to (h,k,l) reflections. The presence of sharp
207 hexant reflections implies coherence between individual layers, and the absence of diffuse
208 diffraction rings is consistent with a lack of turbostratic defects. The latter of which is
209 characteristic of smectitic interlayers.

210 Typical SAED patterns for each sample are presented in Figure 5. Chochołów-06 is the only
211 sample that deviates from the hexagonal single crystal diffraction patterns observed for
212 Chochołów-60, Bukowina Tatrzańska-06 and Bukowina Tatrzańska-41. Chochołów-06 has a
213 well-defined coherence of layers in its mixed-layer crystal particle with varying orientations of

214 these particles around c^* (or Z) producing a slight ring effect, However, one mixed-layer crystal
215 is thick enough to define the dominant single crystal pattern.

216

217 **4.2 High resolution TEM imaging**

218 Lattice fringe images of illite and illite-smectite in samples from Bukowina Tatrzańska-
219 06 and Bukowina Tatrzańska-41 are presented in Figure 6. Bukowina Tatrzańska-06 shows thin
220 illite packets which, based on a 10\AA lattice spacing, are typically around 5 layers and are situated
221 adjacent to I-S packets of similar thickness. Some I-S mixed layers show some lattice defects
222 such as layer terminations (Figure 6a), whilst others are straight crystals (Figure 6b). In
223 comparison, the samples from Bukowina Tatrzańska-41 typically reveal thicker I-S particles of
224 10-15 layers (Figure 6c and d). Here, some diagenetic crystallite packets are terminated against
225 thick illite minerals of, presumably, detrital origin. I-S crystallites show some edge dislocations
226 defined by terminations of layers of illite, probably inherited from highly imperfect, smectite
227 precursor structures. In general, the samples in Figure 6 show substantial I-S growing adjacent to
228 authigenic and detrital illite minerals. These I-S mixed layers display variable lattice
229 morphologies with some collapse structures, detailing the probable prior existence of an
230 expandable smectite component.

231

232 **4.3 Chemistry**

233 Bulk mineralogical data from Chochołów PIG-1 and Bukowina Tatrzańska PIG-1 is
234 synthesized from Środoń et al. (2006b) and Day-Stirrat et al. (2008a) (Table 1). Standard structural
235 formulae for an illite-smectite half-cell and associated elemental concentrations expressed as
236 weight percent oxides are presented in Tables 2 to 5 for Chochołów-06, Chochołów-60, Bukowina
237 Tatrzańska-06, Bukowina Tatrzańska-41, respectively. Both the octahedral totals (range = 1.92 to

238 2.11) and the chemical compositions are within the previously published range for illite-smectite;
239 some K^+ values are outside the range of illite, and even muscovite (>1), and are, therefore,
240 unrealistic and probably related to the noted mobility of potassium under an electron beam (Ahn
241 and Peacor, 1986; Brusewitz, 1986; Ramseyer and Boles, 1986; Środoń et al., 1986; van der Pluijm
242 et al., 1988; Weaver, 1989; Jiang et al., 1990; Li et al., 1997; Hover et al., 1999; Masuda et al.,
243 2001). The Si:Al ratio in the tetrahedral sheet is consistent with illitic material rather than pure
244 mica (Figure 7).

245 In order to compare the chemical composition of I-S from Chochołów-06 (50% I in I-S)
246 with that of the other samples (all 76% I in I-S), the Kolmogorov-Smirnov test is employed as
247 there are not enough data to adequately define averages by arithmetic means. Chochołów-06 has
248 a broader range of tetrahedral Si^{4+} values but includes values which are similar to or lower than
249 those in the more illitic I-S from Chochołów-60 (Figure 8a). Gulf Coast data previously published
250 by Ahn and Peacor (1986a) are presented as a reference frame for progressive illitization and
251 demonstrate the utility of the K-S test; however, it should be noted that these samples are not an
252 analog for the Podhale Basin.

253 The octahedral cation chemistry (Figure 8b and 8c) of Chochołów-06 displays a similar
254 range to that in the more illitic samples from Chochołów-60, albeit with more samples relatively
255 enriched in Fe^{3+} and Mg^{2+} . Total Al^{3+} is reflective of tetrahedral Si^{4+} occupancy and octahedral
256 substitution. The relative difference between sample data is described as a D-Statistic in Table 6.

257 I-S from Bukowina Tatrzańska-41 has a more homogeneous tetrahedral composition and a
258 much more aluminous octahedral composition than Bukowina Tatrzańska-06, which is richer in
259 Fe^{3+} (calculated Kolmogorov-Smirnov D-statistic of 43%; Figure 8f). Furthermore, the octahedral
260 composition of I-S in Bukowina Tatrzańska-41 is much more homogeneous than that in Bukowina
261 Tatrzańska-06. The D-statistic shows that all samples analyzed are statistically different in terms

262 of their octahedral cation compositions. The distributions (Figure 8) and the D-statistics (Table 6)
263 show that Bukowina Tatrzańska-41 has less Fe^{3+} and Mg^{2+} and more Al^{3+} in its octahedral sites
264 than Bukowina Tatrzańska-06.

265

266 **5. Discussion**

267 The composition of I-S reflects both that of the initial detrital supply and also changes
268 resulting from diagenesis, which ultimately transform I-S to illite, and perhaps chlorite and quartz
269 (Hower et al., 1976; Boles and Franks, 1979; Weaver, 1989; van de Kamp, 2008). From a general
270 chemical perspective, the illitization of smectite results in the export of Fe^{3+} (or Fe^{2+}) and Mg^{2+}
271 from I-S to chlorite or perhaps late-diagenetic ankerite, an increase in the concentration of Al^{3+}
272 within illite, and the formation of quartz as the more siliceous smectite is converted to illite. It is
273 commonly understood that Al^{3+} is conserved (Land et al., 1997; Land and Milliken, 2000) within
274 a diagenetic system. Whilst these general trends are well documented, they may be masked in a
275 single case by natural variations in the composition of detrital I-S related to provenance changes.
276 A common provenance and well-documented, progressive and predictable diagenetic trends
277 (Środoń et al., 2006b) makes this dataset from Podhale Basin ideal for high resolution study.
278 Furthermore, illitization of smectite has been documented to play an important role on the
279 development of an oriented alignment of neoformed clay minerals (Day-Stirrat et al., 2008a) in
280 the Podhale Basin.

281 The chemical and mineralogical data presented here show that in the deeper parts of the
282 basin (5000m to 7000m of maximum burial) the rate of smectite illitization has slowed or
283 terminated, such that the % I in I-S does not change further (Table 1). Nevertheless, detailed
284 analysis of I-S chemistry (Figure 6) and morphology (Figure 8) suggests continued
285 recrystallization with increasing depth, observed as an increase in the size and coherency of I-S

286 crystallite packets. In terms of the use of sonic velocity as a method to estimate porosity and pore
287 pressure, the implication of increased preferred orientation and thicker, more coherent I-S packets
288 is increased velocities at a constant porosity and pore fluid pressure.

289 Further, with increasing burial depth, K₂O in the whole rock (Środoń et al., 2006b) is
290 approximately conserved (Table 1). By assuming that K-feldspar contains 15% K⁺ in its structural
291 formula (i.e. 0.1 Na per formula: Środoń, 2009) and assigning an appropriate percentage of the
292 K₂O to K-feldspar, the rest of the K₂O can be assigned to K-bearing 2:1 clays (mica, illite and
293 illite-smectite; Table 1). These calculations show that the K₂O content of the 2:1 clay fraction does
294 not evolve down the profile, staying between 5.6 and 7.4%. This consistency, despite a clear
295 smectite illitization trend, can be explained only by a redistribution of K₂O within the 2:1 fraction
296 (dissolution of detrital illite/mica providing K₂O for neoformed illite). Dissolution of illite with
297 increasing burial depth is probably unreasonable as illite would be in equilibrium with smectite
298 illitization.

299 It is well known that smectite produces concentric ring patterns in SAED associated with
300 turbostratic disorder (Moore and Reynolds, 1997), resulting from the weak mutual attraction
301 between hydrated cations in the interlayer space and adjacent 2:1 layers and the resultant lack of
302 ‘keying’ effects which allows more random layer positioning. XRD indicates that the most
303 diagenetically immature sample in this study contains randomly interstratified (R0) I-S with 50%
304 illite layers (Środoń et al., 2006b), but only limited turbostratic disorder (Figure 5). The nature of
305 the smectite and illite interfaces in interstratified mixed-layered ‘crystallite packets’ can affect
306 SAED patterns (Bell, 1986), as the boundary between smectite and illite layers may be layer
307 terminating, changing the crystal lattice planes on the scale of the electron beam and producing
308 what appears to be small amounts of turbostratic disorder (see Figure 5). The three more
309 diagenetically mature samples contain R1 ordered I-S (Środoń et al., 2006b) with essentially

310 identical (76%) proportions of I in I-S; these samples have correspondingly similar SAED patterns
311 which are also similar to those observed in previous studies of similar material (e.g. Ahn and
312 Peacor, 1986; Jiang et al., 1990). However, the ordering suggested by XRD is not entirely matched
313 by the high resolution TEM observations, which show progressive ordering from Bukowina
314 Tatrzańska-06 to Bukowina Tatrzańska-41 and an increase in crystallite size. This suggests that I-
315 S continues to recrystallize beyond the level implied by XRD data, revealed by TEM because this
316 technique can discern a packet of crystallites within a size fraction, whereas XRD is the average
317 crystallographic response of all the crystallites in that fraction. Small differences in SAED patterns
318 of the three more mature samples most probably relate to (a) the coherency of ‘crystallite packets’,
319 with larger packets producing more clearly identified single crystal patterns (Ahn and Peacor,
320 1986; Li et al., 1997), and (b) the octahedral substitution of Fe^{3+} (or Fe^{2+}) and Mg^{2+} for Al^{3+} in the
321 octahedral layer, with Fe^{3+} being the most significant substitution due to the size of the atom
322 relative to Al^{3+} . The most coherent SAED patterns for I-S are thus seen in Bukowina Tatrzańska-
323 41, which contain, according to lattice fringe images (Figure 6), the thickest I-S crystallites which
324 also have the least Fe^{3+} and Mg^{2+} in the octahedral sheet (Figure 8).

325 It has been previously shown that on a 1mm^2 scale, the preferred orientation of I-S
326 crystallites (Figure 2) in these wells increases substantially during the main phase of illitization
327 (Day-Stirrat et al., 2008a); a similar phenomenon was observed in the Gulf of Mexico by Ho et
328 al. (1999). The change in preferred orientation implies that illitization occurs as a dissolution –
329 reprecipitation reaction and that the neformed mineral grows perpendicular to maximum
330 effective stress (Day-Stirrat et al., 2008a). In the closed system implied by the whole rock
331 chemistry (constant K_2O) and mineralogy of these mudstones (Środoń et al., 2006b), potassium
332 for illite is supplied from K-feldspar, with additional Al^{3+} and Si^{4+} from kaolinite. Changes in the
333 proportion of illite in mixed-layer I-S halt at around 5 km paleo burial depth that is around 100°C

334 (Table 1, Figure 2). More deeply buried samples, such as Bukowina Tatrzańska-41, which has a
335 maximum burial depth of 7.1 km and a maximum paleo-temperature of close to 150°C (Środoń
336 et al., 2006a), have essentially identical % I in I-S. However, in the apparent absence of % I in I-
337 S change, the preferred orientation of I-S in the more deeply buried samples is somewhat higher.
338 These data could imply (a) mechanical rearrangement of phyllosilicates as a result of higher
339 effective stresses; (b) continued recrystallization but with no change in % I within I-S; (c)
340 formation of a variably aligned phyllosilicate fabric during the main phase of illitization, with no
341 further recrystallisation during continued burial.

342 It is highly unlikely that the somewhat enhanced preferred orientation is due to
343 mechanical rearrangement. Firstly, the samples have low porosities and secondly, mercury
344 injection porosimetry data suggest that most pores are smaller than ~ 20 nm (Day-Stirrat et al.,
345 2008a). The lack of physical space precludes substantial mechanical reorientation of particles
346 which are larger than the pores. Given that the diagenetic system here appears to be closed, any
347 change in the microfabric is likely to result in a shift of load from matrix grains to pore fluid, a
348 decrease in effective stress, an argument recently discussed by Goult et al. (2016). Given that
349 the pore volume to matrix volume is weighed heavily in favor of the matrix, any change could
350 have proportionally large effects on pore fluid. Therefore, in high pressure high temperature
351 wells the loading-unloading behavior (Bowers, 1995), decrease in effective stress, may be
352 extremely complex and potentially away from illite compaction trends defined for lower
353 effective stresses (Lahann, 2002; Lahann and Swarbrick, 2011).

354 Unfortunately, our data cannot unequivocally differentiate hypotheses (b) and (c).
355 However, lattice fringe images suggest that I-S crystallite packages in Bukowina Tatrzańska-41
356 are larger than those in Bukowina Tatrzańska-06, implying continuing crystal growth without the
357 destruction of smectite layers in mixed-layer I-S (Figure 6). We infer that the I-S does not

358 become more illitic due to a lack of supply of K^+ , or that residual smectite layers are physically
359 occluded from interacting with cations in solution. A clear compositional difference (Figure 8)
360 between I-S in Bukowina Tatrzańska-06 and Bukowina Tatrzańska-41 supports the idea of
361 continued recrystallization. The octahedral occupancy of I-S in Bukowina Tatrzańska-41 is much
362 more aluminous than that of Bukowina Tatrzańska-06, essentially more mica like, and the
363 overall composition of I-S in Bukowina Tatrzańska-41 is much more homogeneous than that in
364 Bukowina Tatrzańska-06. Stated very simply, Bukowina Tatrzańska-41 has a distribution of
365 illite-smectite chemical formulae that are simplified relative to Bukowina Tatrzańska-06,
366 consistent with the progressive conversion of illite towards a 'mica' at significantly greater
367 temperatures (van de Kamp, 2008).

368 The data in this study, plus those from Środoń et al. (2006b) and Day-Stirrat et al.
369 (2008a), indicate continued recrystallization and export of Fe^{3+} from I-S as, during late
370 diagenesis, it transforms towards a more muscovite-like composition. We propose that this is
371 part of a series of diagenetic steps (Figure 9) that converts a broadly isotropic fabric inherited as
372 a result of the deposition of clay floccules to the highly aligned fabric observed in low grade
373 metamorphic pelites (Haines et al., 2009). Reorientation of the clay fabric is restricted during the
374 main stage of mechanical compaction, during which water is expelled, but is enhanced during the
375 main stage of smectite illitization. In this study, at higher levels of diagenesis, we see that whilst
376 recrystallization of illite continues, there is a limited change in the orientation of the illite fabric.
377 As diagenesis gives way to low grade metamorphism, there is once again a more striking
378 development of an aligned phyllosilicate fabric, reflecting continuing clay mineral
379 recrystallization and growth (Figure 9). Abrupt diagenetic steps are not applicable to all major
380 diagenetic reactions. For example, once quartz cementation reaches a kinetically favorable

381 activation energy (with the presence of a clean quartz surface) and temperature the reaction
382 simply runs until there is no more space for quartz cementation (Taylor et al., 2010).

383

384 **6. Conclusions**

385 TEM-EDS data and statistical tests presented here describe a systematic change in I-S
386 chemistry with increased burial temperature beyond the termination of the smectite to illite
387 transformation. TEM-EDS data is accompanied by SAED patterns that show well defined
388 coherence of layers in I-S packets, single crystal patterns and an absence of turbostratic disorder.
389 Concomitant with this change in mineral formulae is an increase in crystallinity observable in
390 lattice fringe images and a change from high angle contacts between discrete I-S packets to more
391 coalesced crystallites. We propose that the data presented here describe the continued increase in
392 the preferred orientation of I-S beyond the smectite to illite transformation. This involves a change
393 in crystallite chemistry reflected by (a) the progressive removal of Fe^{3+} and Mg^{2+} from the
394 octahedral sheet of I-S, (b) a decrease in crystallite layer rotation and (c) the coalescence of I-S
395 crystallites in a high effective stress regime. We suggest that these relatively subtle changes are
396 one of a series of diagenetic steps which convert chemically diverse I-S with a broadly isotropic
397 phyllosilicate fabric into chemically homogeneous illite with a highly anisotropic fabric in low
398 grade metamorphic rocks. These results have implications for loading-unloading trends in
399 diagenetically mature siliciclastic systems and for predicating porosity and pore pressure from
400 wireline logs.

401 **7. Acknowledgements**

402 We thank the UK Natural Environment Research Council (NERC) and BP for supporting RJD-S's
403 PhD which generated the TEM-EDS data and the EMAL at the University of Michigan for use of
404 their TEM and sample preparation equipment for lattice fringe imaging.

405
406

Table 1 Present day depth [m], maximum burial depth [m], %I in I-S and bulk mineralogy from X-ray diffraction (Środoń et al., 2006b).

	CH-4	CH-6	CH-12	CH-20	CH-23	CH-28	CH-38	CH-44	CH-56	CH-60	CH-66
Sample											
Actual Burial Depth (m)	193	280	514	821	1031	1283	1671	2012	2410	2611	2968
Estimated Maximum Burial Depth [m]	2393	2480	2714	3021	3231	3483	3871	4212	4610	4811	5168
Max. Temp (°C) from modeling	57.5	60	67.5	75	80	85	95	105	115	120	127.5
Quartz	19.0	24.3	18.5	22.9	21.7	20.4	16.3	26.0	20.5	27.5	22.4
K-Feldspar	2.2	2.3	2.2	1.5	1.3	0.5	1.5	1.0	0.5	0.4	0.5
Plagioclase	3.0	5.9	3.7	4.7	3.6	5.7	5.0	7.0	6.5	9.0	6.0
Calcite	7.7	10.2	11.9	10.5	10.0	10.4	0.9	3.7	3.6	13.2	17.0
Dolomite	3.8	5.4	3.5	4.1	4.5	4.7	4.5	6.2	5.2	4.6	6.7
Halite	0.0	0.0	0.0	0.0	0.0	0.0	0.6	0.5	1.2	0.0	0.0
Pyrite	1.5	1.5	1.2	0.7	0.9	2.3	2.3	2.5	1.8	1.2	1.5
Siderite	0.0	0.4	0.3	0.7	0.8	0.0	0.0	0.2	0.0	0.2	0.2
Anatase	0.0	0.0	0.0	0.0	0.2	0.0	0.6	0.4	0.5	0.7	0.5
Kaolinite	3.2	1.5	3.2	3.6	2.9	2.6	1.0	1.0	0.8	0.0	0.0
Illite + Mica + Fe-Smectite	45.8	46.8	50.2	49.2	43.9	49.1	60.8	53.9	60.1	41.1	41.8
Chlorite	0.7	4.0	2.6	2.1	2.6	3.6	7.4	5.2	4.8	4.7	4.2
Total clay	49.7	52.3	56.0	54.9	49.4	55.3	69.2	60.1	65.7	45.8	46.0
%S in I/S	52	50	63	47	45	44	24	32	27	24	31
Ordering	0	0	0	0	0/1	0/1	1	1	1	1	1
K2O (%)	3.6	3.6	3.2	3.0	2.9	3.0	4.7	3.4	4.2	2.9	2.9
K-Bearing 2:1 clays	22.0	23.4	18.6	26.1	24.1	27.5	46.2	36.7	43.9	31.2	28.8
K ₂ O in Illite Wt.%	2.4	2.3	2.2	2.3	2.3	2.8	3.6	2.9	3.9	2.7	2.7
% K ₂ O in Illite	9.1	10.0	8.6	11.4	10.3	9.9	12.7	12.7	11.2	11.5	10.8
K ₂ O/K-Feldspar	1.6	1.5	1.5	2.0	2.2	6.0	3.1	3.4	8.5	7.3	5.8
TEM Study Samples And %I in I-S		CH-6 50%								CH-60 76%	
Sample	BKT-1	BKT-6	BKT-12	BKT-17	BKT-23	BKT-28	BKT-35	BKT-41			
Actual Burial Depth (m)	102	294	611	903	1261	1595	1904	2201			
Estimated Maximum Burial Depth [m]	4908	5100	5417	5709	6067	6401	6710	7007			
Max. Temp (°C) from modeling	103	107	114	120	127	134	141	147			
Quartz	26.6	25.2	27.0	24.1	23.3	27.0	29.4	26.4			
K-Feldspar	0.8	0.5	1.0	0.5	1.0	0.0	0.5	0.0			
Plagioclase	7.1	6.8	6.6	5.3	4.5	6.2	6.3	5.7			
Calcite	9.5	7.3	5.4	6.9	6.1	11.2	0.8	8.8			
Dolomite	7.5	6.5	7.6	6.9	7.8	5.5	6.2	4.2			
Halite	0.0	0.0	0.0	0.5	0.0	0.0	0.5	1.0			
Pyrite	0.9	0.9	1.2	1.3	1.0	1.5	2.4	3.0			
Siderite	0.0	0.5	0.0	0.0	0.0	0.0	0.0	0.0			
Anatase	0.5	0.5	0.5	0.5	0.4	0.4	0.5	0.3			
Kaolinite	0.8	0.5	0.0	0.0	0.0	0.0	0.0	0.0			
Illite + Mica + Fe-Smectite	53.6	54.3	52.0	48.1	50.7	46.8	50.1	51.5			
Chlorite	5.6	5.6	6.1	3.1	4.2	4.4	3.6	4.0			
Total clay	60.0	60.4	58.1	51.2	54.9	51.2	53.7	55.5			
%S in I/S	25	24	26	25	20	30	18	24			
Ordering	1	1	1	1	1	1	1	1			
K ₂ O (%)	3.5	3.6	3.1	3.3	3.3	3.1	3.4	3.3			
K-Bearing 2:1 clays	40.2	41.3	38.5	36.1	40.6	32.8	41.1	39.1			
K ₂ O in Illite Wt.%	3.1	3.3	2.6	3.1	2.8	3.1	3.1	3.3			
% K ₂ O in Illite	13.1	12.6	14.6	11.8	14.5	10.6	13.1	11.9			
K ₂ O/K-Feldspar	4.4	7.1	3.1	6.6	3.3		6.8				
TEM Study Samples And %I in I-S		BKT-6 76%						BKT-41 76%			

407
408
409
410
411
412

413
414
415

Table 2: Chochołów-06 structural formulae for a half cell and associated elemental concentrations expressed as wt.% oxides normalized to 95%.(Merriman et al., 1995), 50 % illite in illite-smectite.

	E001	E003	E005	E009	E011	E019
Si	3.31	3.65	3.12	3.56	3.12	3.59
Al	0.69	0.35	0.88	0.44	0.88	0.41
Tet. Sum	4.00	4.00	4.00	4.00	4.00	4.00
Al	1.93	1.77	1.47	1.59	1.73	1.61
Fe	0.07	0.07	0.20	0.14	0.07	0.15
Mg	0.00	0.10	0.23	0.28	0.19	0.20
Ti	0.01	0.02	0.02	0.00	0.03	0.00
Oct. Sum	2.01	1.96	1.92	2.01	2.02	1.96
Ca	0.00	0.02	0.00	0.02	0.01	0.03
K	0.68	0.52	1.34	0.66	0.95	0.67
Inter. Sum	0.68	0.54	1.34	0.68	0.96	0.70
SiO ₂	50.24	57.21	44.78	54.52	46.67	0.69
Al ₂ O ₃	33.77	28.18	28.50	26.23	33.08	33.08
TiO ₂	0.17	0.47	0.41	0.35	0.69	0.15
Fe ₂ O ₃	1.37	1.46	3.72	2.88	1.37	11.15
MgO	1.24	1.01	2.24	2.88	1.88	46.67
CaO	0.16	0.24	0.33	0.28	0.15	1.88
K ₂ O	8.05	6.43	15.04	7.86	11.15	1.37
Total	95	95	95	95	95	95
	E021	E024	E026	E028	E030	
Si	3.50	3.44	3.32	3.26	3.04	
Al	0.50	0.56	0.68	0.74	0.96	
Tet. Sum	4.00	4.00	4.00	4.00	4.00	
Al	1.48	1.63	1.62	1.69	1.55	
Fe	0.24	0.18	0.15	0.19	0.20	
Mg	0.25	0.16	0.14	0.09	0.33	
Ti	0.03	0.02	0.01	0.03	0.02	
Oct. Sum	2.00	1.99	1.92	2.00	2.10	
Ca	0.19	0.02	0.25	0.01	0.09	
K	0.34	0.66	0.55	0.76	0.82	
Inter. Sum	0.53	0.68	0.80	0.77	0.91	
SiO ₂	54.05	52.54	50.58	49.26	45.07	
Al ₂ O ₃	25.88	28.45	29.69	31.16	31.59	
TiO ₂	0.63	0.49	0.15	0.59	0.36	
Fe ₂ O ₃	5.02	3.64	3.12	3.89	3.85	
MgO	2.57	1.62	1.39	0.92	3.27	
CaO	2.72	0.34	3.54	0.16	1.31	
K ₂ O	4.14	7.91	6.53	9.02	9.56	
Total	95	95	95	95	95	

416
417

Table 3: Chochołów-60 structural formulae for a half cell and associated elemental concentrations expressed as wt.% oxides normalized to 95%.(Merriman et al., 1995), 76 % illite in illite-smectite.

	J001	J009	J011	J013	J015	J017	J019	J021
Si	3.32	3.28	3.47	3.37	3.25	3.12	3.19	3.37
Al	0.68	0.72	0.53	0.63	0.75	0.88	0.81	0.63
Tet. Sum	4.00	4.00	4.00	4.00	4.00	4.00	4.00	4.00
Al	1.81	1.78	1.53	1.80	1.67	1.45	1.72	1.93
Fe	0.10	0.14	0.17	0.08	0.16	0.21	0.17	0.10
Mg	0.14	0.07	0.21	0.05	0.10	0.31	0.01	0.01
Ti	0.02	0.01	0.03	0.01	0.05	0.02	0.02	0.01
Oct. Sum	2.07	2.00	1.94	1.94	1.98	1.99	1.92	2.05
Ca	0.05	0.07	0.11	0.07	0.06	0.05	0.09	0.04
K	0.49	0.62	0.65	0.70	0.76	1.13	0.89	0.45
Inter. Sum	0.54	0.69	0.76	0.77	0.82	1.18	0.98	0.49
SiO ₂	51.62	50.26	52.81	51.63	49.02	45.41	47.59	52.78
Al ₂ O ₃	32.71	32.45	26.64	31.63	31.04	28.69	32.11	33.99
TiO ₂	0.48	0.23	0.62	0.26	0.92	0.33	0.32	0.12
Fe ₂ O ₃	2.00	2.94	3.42	1.59	3.16	3.99	3.28	2.05
MgO	1.48	0.76	2.19	0.53	1.00	3.07	0.08	0.06
CaO	0.77	0.95	1.54	0.96	0.84	0.67	1.20	0.52
K ₂ O	5.94	7.42	7.79	8.41	9.02	12.84	10.42	5.48
Total	95	95	95	95	95	95	95	95

418
419
420
421
422
423
424
425
426
427
428
429
430
431
432
433
434
435
436
437
438
439
440
441
442
443
444

445 Table 4: Bukowina Tatrzańska-06 structural formulae for a half cell and associated elemental concentrations expressed
 446 as wt.% oxides normalized to 95%.(Merriman et al., 1995), 76 % illite in illite-smectite.

	H003	H007	H009	H011	H013	H018	H022
Si	3.36	3.22	3.38	3.52	3.32	3.42	3.26
Al	0.64	0.78	0.62	0.48	0.68	0.58	0.74
Tet. Sum	4.00	4.00	4.00	4.00	4.00	4.00	4.00
Al	1.66	1.32	1.68	1.66	1.76	1.76	1.72
Fe	0.20	0.34	0.18	0.12	0.14	0.07	0.14
Mg	0.22	0.28	0.03	0.16	0.07	0.17	0.05
Ti	0.00	0.02	0.01	0.00	0.01	0.01	0.01
Oct. Sum	2.08	1.96	1.90	1.94	1.98	2.01	1.92
Ca	0.19	0.00	0.03	0.04	0.00	0.01	0.06
K	0.22	1.18	0.91	0.73	0.80	0.71	0.89
Inter. Sum	0.41	1.18	0.94	0.77	0.80	0.72	0.95
SiO ₂	52.40	46.43	50.66	53.39	50.30	52.61	48.84
Al ₂ O ₃	30.52	25.62	29.21	27.60	31.49	30.38	31.35
TiO ₂	0.03	0.32	0.16	0.53	0.21	0.25	0.28
Fe ₂ O ₃	4.19	6.50	3.54	2.50	2.76	1.34	2.84
MgO	2.31	2.70	0.30	1.61	0.71	1.73	0.49
CaO	2.81	0.04	0.41	0.63	0.01	0.14	0.78
K ₂ O	2.75	13.39	10.71	8.75	9.51	8.55	10.42
Total	95	95	95	95	95	95	95
	H024	H026	H028	H030	H032	H034	
Si	3.17	3.39	3.07	3.39	3.10	3.46	
Al	0.83	0.61	0.93	0.61	0.90	0.54	
Tet. Sum	4.00	4.00	4.00	4.00	4.00	4.00	
Al	1.49	1.54	1.04	1.58	1.44	1.53	
Fe	0.22	0.26	0.56	0.19	0.22	0.15	
Mg	0.24	0.15	0.29	0.16	0.31	0.23	
Ti	0.00	0.05	0.06	0.02	0.05	0.02	
Oct. Sum	1.95	2.00	1.95	1.95	2.02	1.93	
Ca	0.10	0.07	0.22	0.01	0.04	0.00	
K	1.01	0.55	0.89	0.90	1.02	0.94	
Inter. Sum	1.11	0.62	1.11	0.91	1.06	0.94	
SiO ₂	46.54	51.70	43.80	50.73	45.44	51.93	
Al ₂ O ₃	28.87	27.72	23.78	27.82	28.98	26.28	
TiO ₂	0.00	1.08	1.05	0.36	0.97	0.43	
Fe ₂ O ₃	4.28	5.36	10.67	3.88	4.34	2.94	
MgO	2.38	1.55	2.77	1.56	3.01	2.36	
CaO	1.30	0.96	2.95	0.14	0.53	0.07	
K ₂ O	11.63	6.63	9.98	10.52	11.72	10.99	
Total	95	95	95	95	95	95	

447

448
449

Table 5: Bukowina Tatrzańska-41 structural formulae for a half cell and associated elemental concentrations expressed as wt.% oxides normalized to 95% (Merriman et al., 1995). 76 % illite in illite-smectite.

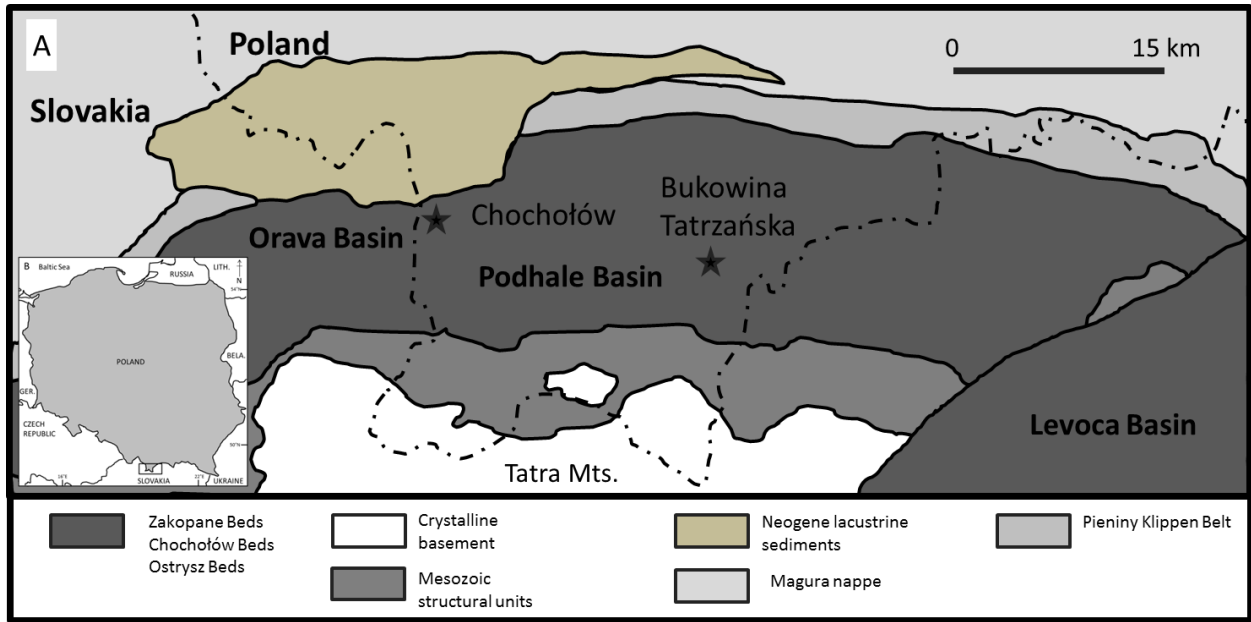
	C003	C005	C007	C010	C012	C014	C016	C018
Si	3.28	3.24	3.22	3.52	3.38	3.28	3.47	3.40
Al	0.72	0.76	0.78	0.48	0.62	0.72	0.53	0.60
Tet. Sum	4.00	4.00	4.00	4.00	4.00	4.00	4.00	4.00
Al	1.77	1.88	1.94	1.50	1.76	1.79	1.58	1.62
Fe	0.11	0.04	0.07	0.07	0.10	0.09	0.17	0.14
Mg	0.19	0.00	0.10	0.35	0.18	0.02	0.13	0.19
Ti	0.01	0.01	0.00	0.07	0.02	0.01	0.03	0.03
Oct. Sum	2.08	1.93	2.11	1.99	2.06	1.91	1.91	1.98
Ca	0.00	0.10	0.03	0.16	0.00	0.00	0.02	0.00
K	0.67	0.75	0.47	0.45	0.58	0.97	0.86	0.82
Inter. Sum	0.67	0.85	0.50	0.61	0.58	0.97	0.88	0.82
SiO ₂	49.83	49.19	50.14	54.44	52.31	49.30	52.21	51.39
Al ₂ O ₃	32.18	34.07	35.93	26.10	31.27	31.95	27.07	28.55
TiO ₂	0.19	0.26	0.11	1.41	0.35	0.23	0.66	0.69
Fe ₂ O ₃	2.27	0.81	1.52	1.52	2.13	1.88	3.40	2.75
MgO	1.94	0.27	1.00	3.64	1.90	0.16	1.27	1.91
CaO	0.63	1.43	0.50	2.38	0.05	0.02	0.23	0.01
K ₂ O	7.96	8.97	5.79	5.52	6.99	11.45	10.17	9.69
Total	95	95	95	95	95	95	95	95

450
451
452
453
454
455
456
457
458
459
460
461
462
463
464
465
466
467
468
469
470
471
472
473
474
475
476

477 Table 6. Summary of the difference using the Kolmogorov-Smirnov test between samples in the Podhale Basin
 478 (ND=no data).

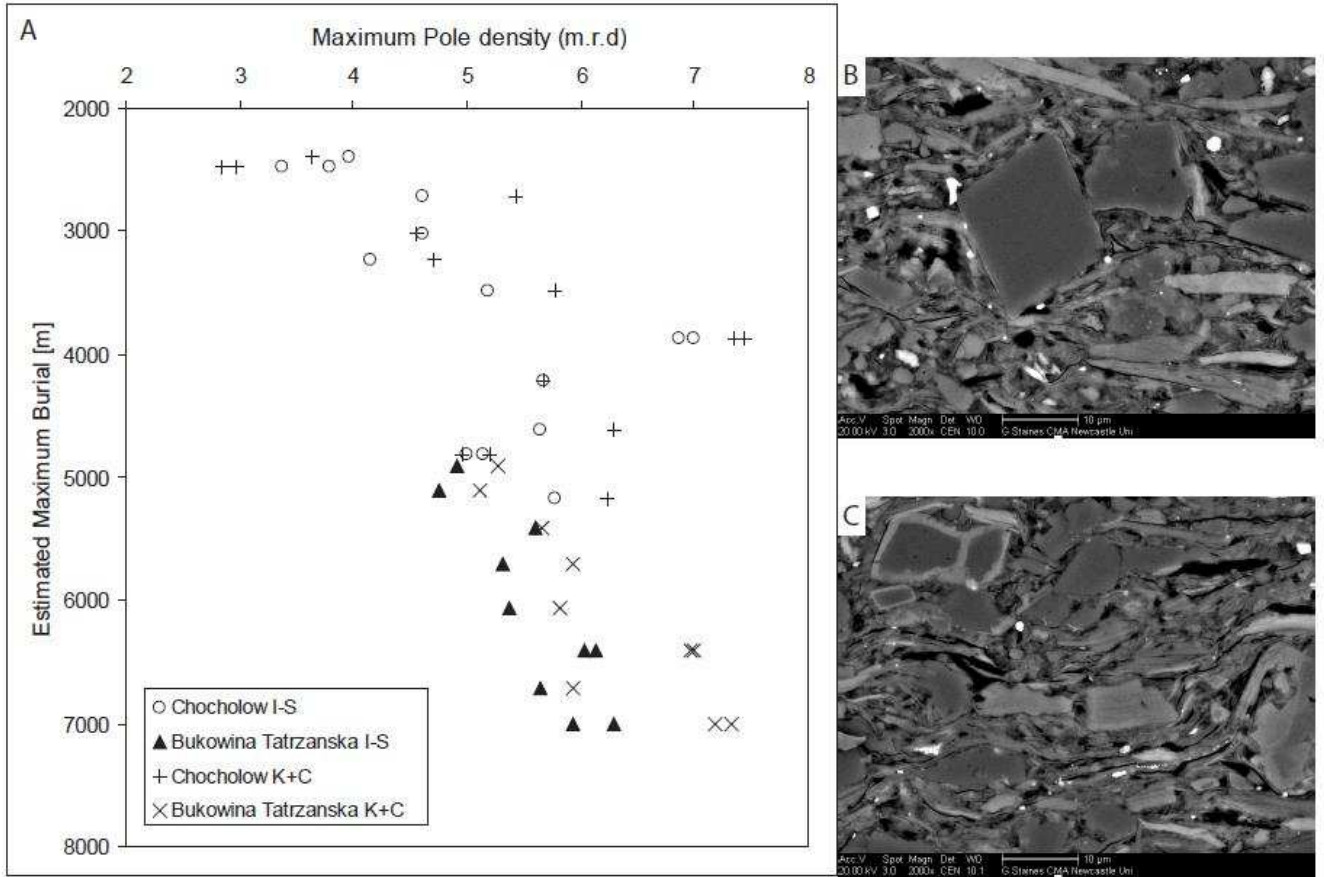
Well and Sample	Difference in Fabric Intensity [m.r.d.]	Difference in % I in I-S	Difference in Octahedral Fe D-Statistic	Difference in Octahedral Mg D-Statistic	Difference in Total Al D-Statistic	Difference in Tetrahedral Si D-Statistic
20% I in I-S and 80% I in I-S (Ahn and Peacor, 1986)	ND	60	75	76	88	100
Chochołów-06 and Chochołów-60	1.48	26	45	40	28	30
Bukowina Tatrzańska-06 and Bukowina Tatrzańska-41	1.2	0	43	30	18	18
Chochołów-06 and Bukowina Tatrzańska-06	0.25	26	37	10	5	8
Chochołów-06 and Bukowina Tatrzańska-41	2.53	26	50	27	18	25
Chochołów-60 and Bukowina Tatrzańska-06	0.32	0	40	48	23	27
Chochołów-60 and Bukowina Tatrzańska-41	0.95	0	39	23	4	25

479
 480
 481
 482
 483
 484
 485
 486
 487
 488
 489
 490
 491
 492
 493
 494
 495
 496
 497
 498
 499
 500
 501
 502
 503
 504
 505
 506
 507
 508



510

511 Figure 1. A: The Podhale Basin with its surrounding sub-basins, and the locations of the Chochotów PIG-1 and
 512 Bukowina Tatrzańska PIG-1 wells (adapted from Środoń et al., 2006b).
 513

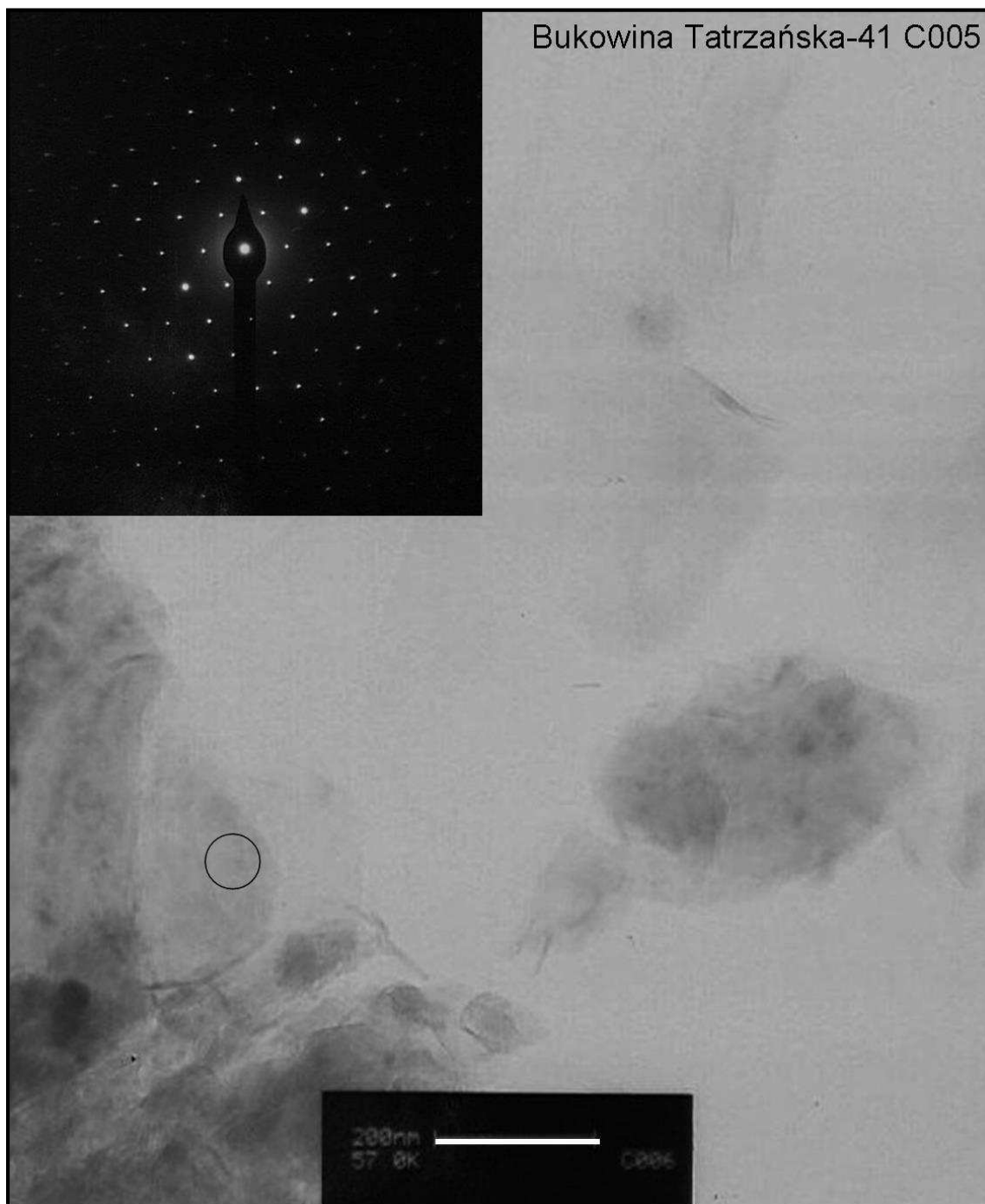


514
 515 Figure 2. (A) Maximum pole density (m.r.d.) for illite-smectite and kaolinite + chlorite for samples from the Podhale
 516 Basin (Day-Stirrat et al, 2008a). Backscattered electron images (B) and (C) of samples at 2480m and 4610m (see Day-
 517 Stirrat et al, 2008a for more images). Smectite illitization appears to terminate at around 4500 m of maximum burial.

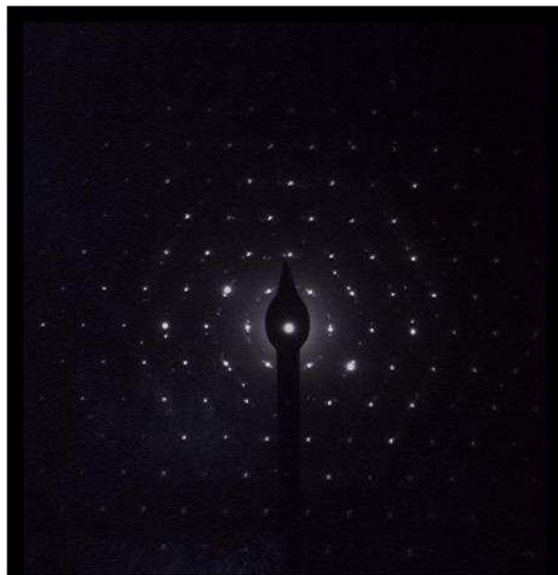


518
519
520
521
522
523
524

Figure 3. Sample Bukowina Tatrzańska-06 H013 (TEM-EDS data in Table 4). Euhedral grain drop-cast on a carbon film-supported 200-mesh copper grid with c^* (Z) parallel to the electron beam. The scale bar is 200nm and the location of diffraction aperture is schematically noted by the ring. The Selected Area Diffraction Pattern (inset) shows a strong hexanet of discrete spots free from distortions or rings that are indicative of turbostratic layering.



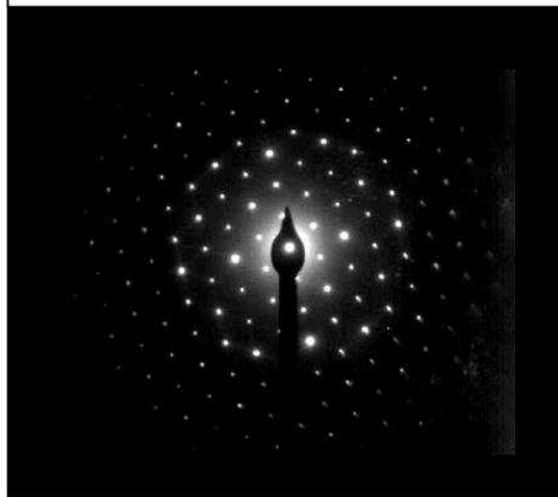
525
526 Figure 4. A grain in sample Bukowina Tatrzańska-41 C005 (TEM-EDS data in Table 5). Grain drop-cast on a carbon
527 film-supported 200-mesh copper grid with c^* (Z) parallel to the electron beam. The scale bar is 200nm and the location
528 of diffraction aperture is schematically noted by the ring. The Selected Area Diffraction Pattern (inset) shows a strong
529 hexanet of discrete spots free from distortions or rings that are indicative of turbostratic layering.
530
531



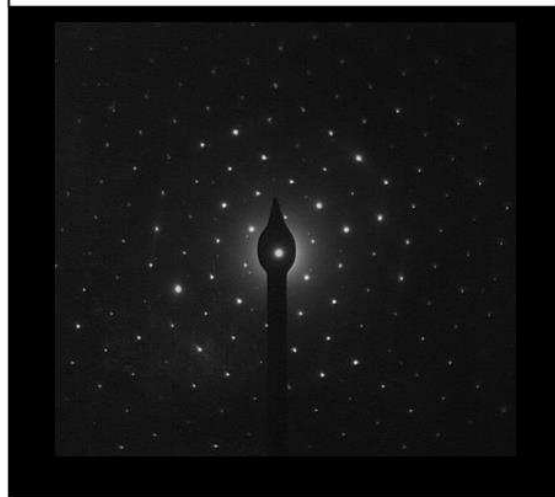
Chochółów-06 E026



Bukowina Tatrzańska-06 H022



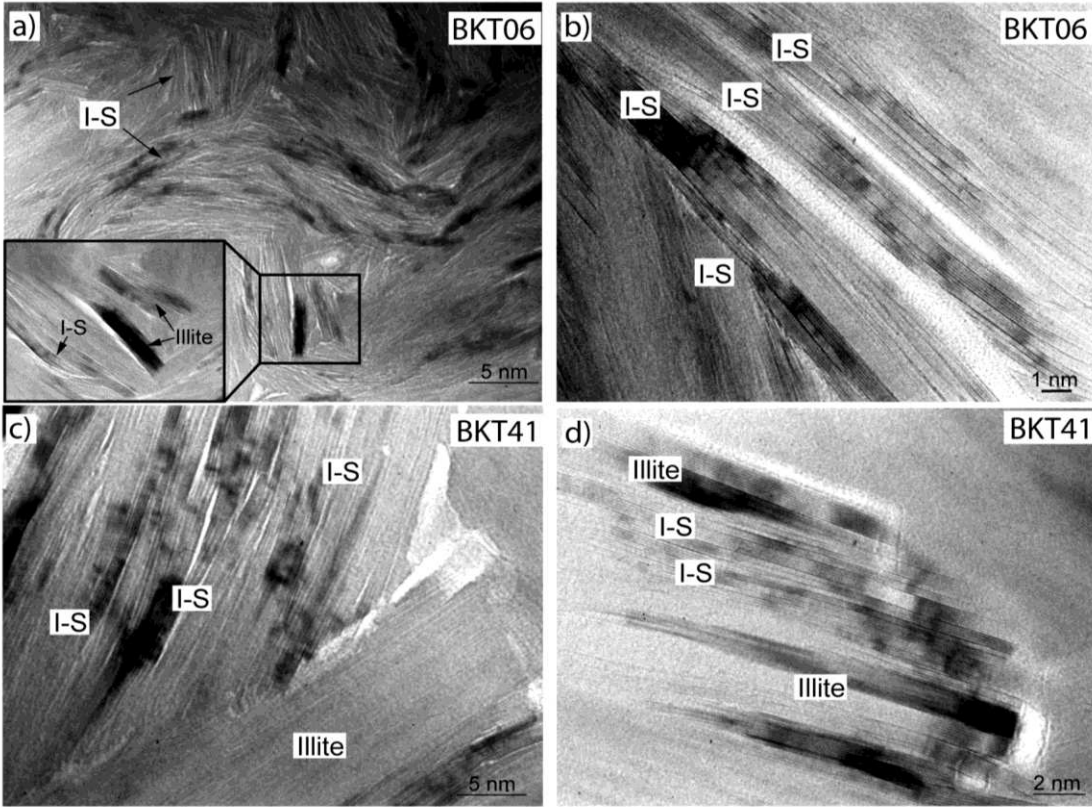
Chochółów-60 J011



Bukowina Tatrzańska-41 C014

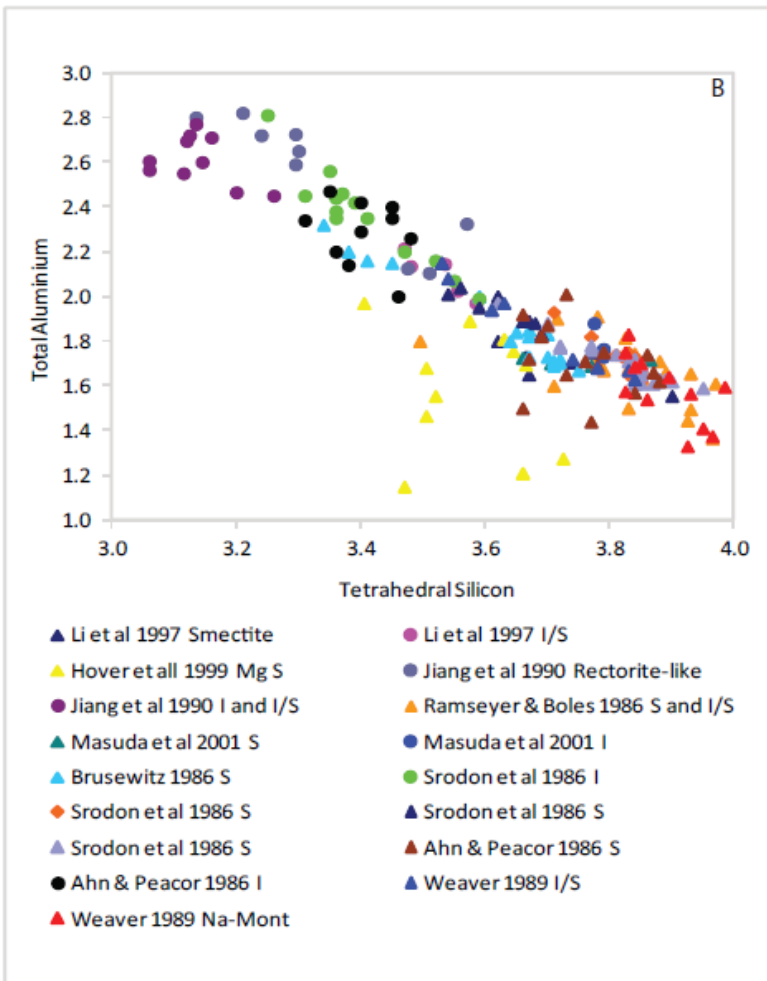
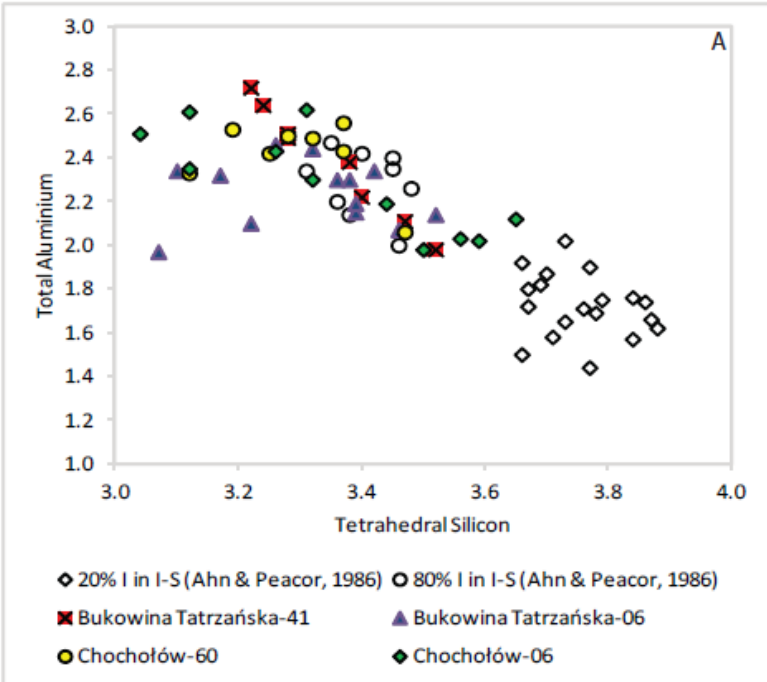
532
533
534
535
536
537
538

Figure 5. Representative Selected Area Diffraction Patterns for samples Chochółów-06, Chochółów-60, Bukowina Tatrzańska-06 and Bukowina Tatrzańska-41 (Tables 2, 3, 4 and 5 for mineral formulae). Chochółów-06 shows well defined coherence of layers in packets with varying orientations, but with one packet that is thick enough to produce a hexagonal single crystal pattern. Chochółów-60, Bukowina Tatrzańska-06 and Bukowina Tatrzańska-41 have Selected Area Diffraction Patterns for (h,k,0) showing well-defined single crystal patterns.

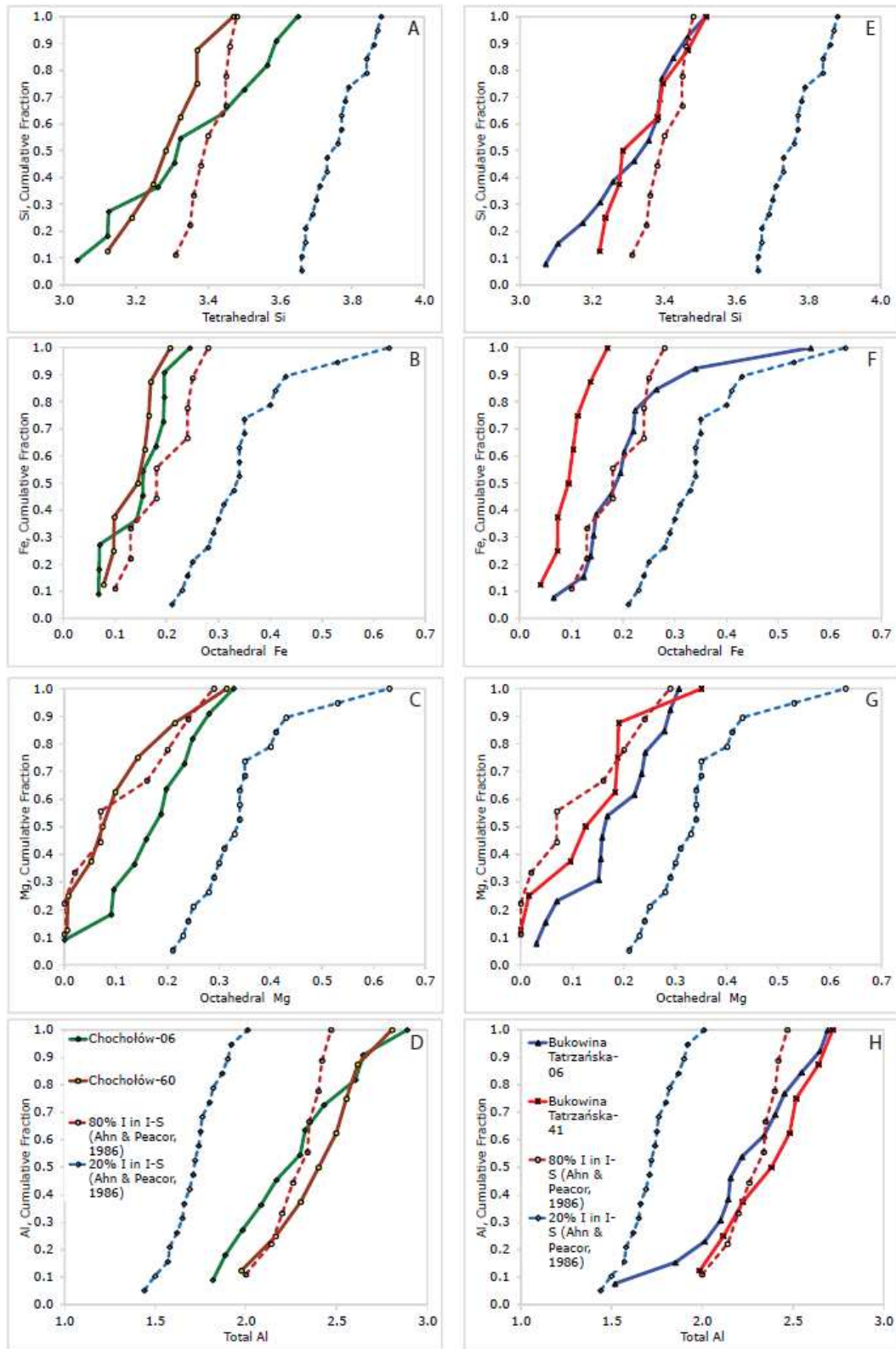


539
 540
 541
 542
 543
 544
 545
 546
 547

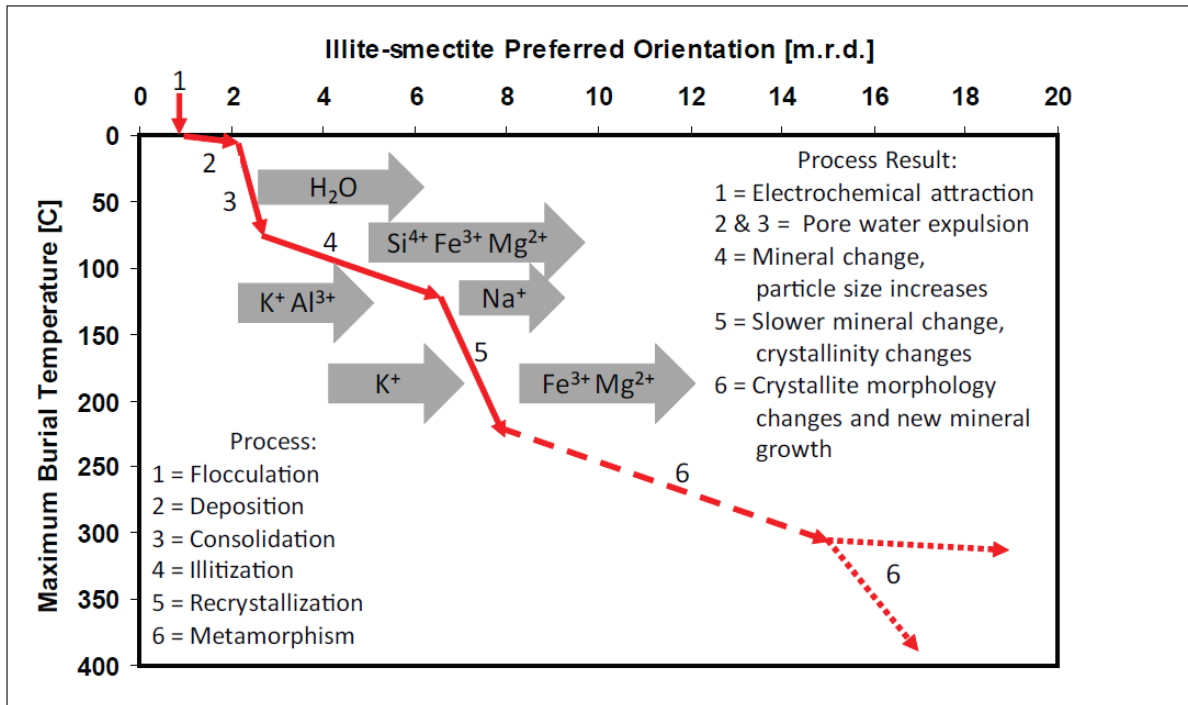
Figure 6. Lattice fringe images of samples Bukowina Tatrzańska-06 and Bukowina Tatrzańska-41 at varying magnifications. A) Thin illite packets growing within illite-smectite (I-S) layers, illite is not continuous with I-S. Layer terminations can be seen in the inset figure, where the arrow pointing to I-S lines on a layer termination B) I-S packets are not continuous and packets are oriented at large angles to each other, C) I-S packets terminate against a thick illite packet (detrital in origin), white areas separating I-S packets are probably indicative of smectite collapse and here may be viewed as porosity at the angstrom scale, D) illite growing within I-S layers, illite packets generally more coherent than I-S.



549 Figure 7. (A) Tetrahedral Si^{4+} versus total Al^{3+} for Chochołów-06, Chochołów-60, Bukowina Tatrzańska-06 and
550 Bukowina Tatrzańska-41 from TEM-EDS, data from Ahn and Peacor (1986a) are also shown. (B) Tetrahedral Si
551 versus total Al from the noted literature sources. Data are from a variety of techniques; Atomic absorption
552 Spectroscopy, DC Plasma-Emission Spectroscopy, Ignited weights, X-ray fluorescence and not TEM-EDS alone. The
553 division of the data into illite (I), illite-smectite (I/S), and smectite (S) is based on the individual author's descriptions.



554
 555 Figure 8. Kolmogorov-Smirnov distributions of (a,e) tetrahedral Si, (b,f) octahedral Fe, (c,g) octahedral Mg and (d,h)
 556 Total Al for comparisons of Chochółów-6 with Chochółów-60 and Bukowina Tatrzańska-06 with Bukowina
 557 Tatrzańska-41. Data from Ahn and Peacor (1986a) for the Texas Gulf Coast are also shown to show the separation of
 558 the data and, therefore, their difference.



559
560 Figure 9. The development of illite-smectite preferred orientation is a stepwise process (Modified from Haines et al.
561 2009). Mechanical processes give way to chemical processes that see initial significant changes in mineralogy and
562 associated preferred orientation. As reaction products are consumed diagenesis slows but potassium is still taken up
563 by clay minerals that concomitantly release iron and aluminum (mica formation). A second significant stage of
564 preferred orientation development occurs into metamorphism but is not well defined.

565
566
567
568
569
570
571
572
573
574
575
576
577
578
579
580
581
582
583
584
585
586
587

588 **8. References**

- 589 Ahn, J.H. and Peacor, D.R., 1986. Transmission and analytical electron microscopy of the
590 smectite to illite transition. *Clays and Clay Minerals*, 34: 165-179.
- 591 Anczkiewicz, A., 2006. Verification by AFT technique of the maximum palaeotemperatures
592 evaluated from illite-smectite for the Tatra Mts., the Podhale Basin and the neighbouring
593 area of the Outer Carpathians. PhD thesis, Institute of Geological Sciences PAN, Krakow
594 (in Polish).
- 595 Aplin, A.C., Matenaar, I.F., McCarty, D.K. and van der Pluijm, B.A., 2006. Influence of
596 mechanical compaction and clay mineral diagenesis on the microfabric and pore-scale
597 properties of deep-water Gulf of Mexico mudstones. *Clays and Clay Minerals*, 54(4):
598 500-514.
- 599 Bell, T.E., 1986. Microstructure in mixed-layer illite/smectite and its relationship to the reaction
600 of smectite and illite. *Clays and Clay Minerals*, 34(2): 146-154.
- 601 Bjørlykke, K. and Høeg, K., 1997. Effects of burial diagenesis on stresses, compaction and fluid
602 flow in sedimentary basins. *Marine and Petroleum Geology*, 14(3): 267-276.
- 603 Boles, J.R. and Franks, S.G., 1979. Clay diagenesis in Wilcox Sandstones of southwest Texas.
604 *Journal of Sedimentary Petrology*, 49: 55-70.
- 605 Bowers, G.L., 1995. Pore Pressure Estimation From Velocity Data: Accounting for Overpressure
606 Mechanisms Besides Undercompaction. *Society of Petroleum Engineers (SPE 27488)*,
607 10(2): 89-95.
- 608 Brusewitz, A.M., 1986. Chemical and Physical-Properties of Paleozoic Potassium Bentonites
609 from Kinnekulle, Sweden. *Clays and Clay Minerals*, 34(4): 442-454.
- 610 Cliff, G. and Lorimer, G.W., 1975. Quantitative-Analysis of Thin Specimens. *Journal of*
611 *Microscopy-Oxford*, 103(MAR): 203-207.
- 612 Curtis, C.D., Lipshie, S.R., Oertel, G. and Pearson, M.J., 1980. Clay Orientation in Some Upper
613 Carboniferous Mudrocks, Its Relationship to Quartz Content and Some Inferences About
614 Fissility, Porosity and Compactional History. *Sedimentology*, 27(3): 333-339.
- 615 Day-Stirrat, R.J., Aplin, A.C., Środoń, J. and van der Pluijm, B.A., 2008a. Diagenetic
616 reorientation of phyllosilicate minerals in Paleogene mudstones of the Podhale Basin,
617 southern Poland. *Clays and Clay Minerals*, 56(1): 100-111.
- 618 Day-Stirrat, R.J., Loucks, R.G., Milliken, K.L., Hillier, S. and van der Pluijm, B.A., 2008b.
619 Phyllosilicate orientation demonstrates early timing of compactional stabilization in
620 calcite-cemented concretions in the Barnett Shale (Late Mississippian), Fort Worth Basin,
621 Texas (U.S.A). *Sedimentary Geology*, 208(1-2): 27-35.
- 622 Day-Stirrat, R.J. et al., 2011. Preferred orientation of phyllosilicates: Effects of composition and
623 stress on resedimented mudstone microfabrics. *Journal of Structural Geology*, 33: 1347-
624 1358.
- 625 Djéran-Maigre, I., Tessier, D., Grunberger, D., Velde, B. and Vasseur, G., 1998. Evolution of
626 microstructures and of macroscopic properties of some clays during experimental
627 compaction. *Marine and Petroleum Geology*, 15(2): 109-128.
- 628 Goult, N.R. and Sargent, C., 2016. Compaction of diagenetically altered mudstones – Part 2:
629 Implications for pore pressure estimation. *Marine and Petroleum Geology*, 77: 806-818.
- 630 Goult, N.R., Sargent, C., Andras, P. and Aplin, A.C., 2016. Compaction of diagenetically
631 altered mudstones – Part 1: Mechanical and chemical contributions. *Marine and*
632 *Petroleum Geology*, 77: 703-713.
- 633 Haines, S.H., van der Pluijm, B.A., Ikari, M.J., Saffer, D.M. and Marone, C., 2009. Clay fabric
634 intensity in natural and artificial fault gouges: Implications for brittle fault zone processes

635 and sedimentary basin clay fabric evolution. *Journal of Geophysical Research-Solid*
636 *Earth*, 114.

637 Ho, N.C., Peacor, D.R. and van der Pluijm, B.A., 1995. Reorientation Mechanisms of
638 Phyllosilicates in the Mudstone-to-Slate Transition at Lehigh Gap, Pennsylvania. *Journal*
639 *of Structural Geology*, 17(3): 345-356.

640 Ho, N.C., Peacor, D.R. and van der Pluijm, B.A., 1999. Preferred Orientation of Phyllosilicates
641 in Gulf Coast Mudstones and Relation to the Smectite-Illite Transition. *Clays and Clay*
642 *Minerals*, 47(4): 495-504.

643 Hover, V.C., Walter, L.M., Peacor, D.R. and Martini, A.M., 1999. Mg-Smectite Authigenesis in
644 a Marine Evaporite Environment, Salina Ometepe, Baja California. *Clays and Clay*
645 *Minerals*, 47(3): 252-268.

646 Hower, J., Eslinger, E.V., Hower, M.E. and Perry, E.A., 1976. Mechanism of Burial
647 Metamorphism of Argillaceous Sediment 1. Mineralogical and Chemical Evidence.
648 *Geological Society of America Bulletin*, 87(5): 725-737.

649 Inoue, A., Kohyama, N., Kitagawa, R. and Watanabe, T., 1987a. Chemical and morphological
650 evidence for the conversion of smectite to illite. *Clays and Clay Minerals*, 42: 276-287.

651 Inoue, A., Velde, B., Meunier, A. and Touchard, G., 1987b. Mechanism of illite formation
652 during smectite-to-illite conversion in a hydrothermal system. *American Mineralogist*,
653 73: 1325-34.

654 Jacob, G., Kisch, H.J. and van der Pluijm, B.A., 2000. The relationship of phyllosilicate
655 orientation, X-ray diffraction intensity ratios, and c/b fissility ratios in metasedimentary
656 rocks of the Helvetic zone of the Swiss Alps and the Caledonides of Jamtland, central
657 western Sweden. *Journal of Structural Geology*, 22(2): 245-258.

658 Jiang, W.T., Peacor, D.R., Merriman, R.J. and Roberts, B., 1990. Transmission and Analytical
659 Electron-Microscopic Study of Mixed-Layer Illite Smectite Formed as an Apparent
660 Replacement Product of Diagenetic Illite. *Clays and Clay Minerals*, 38(5): 449-468.

661 Jiang, W.T., Peacor, D.R. and Buseck, P.R., 1994. Chlorite geothermometry?-contamination and
662 apparent octahedral vacancies. *Clays and Clay Minerals*, 42(5): 593-605.

663 Kim, J., Dong, H.L., Seabaugh, J., Newell, S.W. and Eberl, D.D., 2004. Role of microbes in the
664 smectite-to-illite reaction. *Science*, 303(5659): 830-832.

665 Kim, J.W., Peacor, D.R., Tessier, D. and Elsass, F., 1995. A Technique for Maintaining Texture
666 and Permanent Expansion of Smectite Interlayers for TEM Observations. *Clays and Clay*
667 *Minerals*, 43(1): 51-57.

668 Klimentidis, R.E. and Mackinnon, I.D.R., 1986. High-Resolution Imaging of Ordered Mixed-
669 Layer Clays. *Clays and Clay Minerals*, 34(2): 155-164.

670 Lahann, R., 2002. Impact of smectite diagenesis on compaction modeling and compaction
671 equilibrium. In: A.R. Huffman and G.L. Bowers (Editors), *American Association of*
672 *Petroleum Geologists Memoir 76: Pressure regimes in sedimentary basins and their*
673 *prediction*. American Association of Petroleum Geologists, Tulsa, Oklahoma, pp. 61-72.

674 Lahann, R.W. and Swarbrick, R.E., 2011. Overpressure generation by load transfer following
675 shale framework weakening due to smectite diagenesis. *Geofluids*, 11(4): 362-375.

676 Land, L.S., Mack, L.E., Milliken, K.L. and Lynch, F.L., 1997. Burial diagenesis of argillaceous
677 sediment, south Texas Gulf of Mexico sedimentary basin: A reexamination. *Geological*
678 *Society of America Bulletin*, 109(1): 2-15.

679 Land, L.S. and Milliken, K.L., 2000. Regional loss of SiO₂, and gain of K₂O during burial
680 diagenesis of Gulf Coast mudrocks, USA. In: R.H. Worden and S. Morad (Editors),

- 681 Quartz Cementation in Sandstones. International Association of Sedimentologists, pp.
682 183-197.
- 683 Li, G.J., Peacor, D.R. and Coombs, D.S., 1997. Transformation of smectite to illite in bentonite
684 and associated sediments from Kaka Point, New Zealand: Contrast in rate and
685 mechanism. *Clays and Clay Minerals*, 45(1): 54-67.
- 686 Marynowski, L. et al., 2006. Origin of organic matter from tectonic zones in the Western Tatra
687 Mountains Crystalline Basement, Poland: An example of bitumen - source rock
688 correlation. *Marine and Petroleum Geology*, 23(2): 261-279.
- 689 Masuda, H., Peacor, D.R. and Dong, H., 2001. Transmission electron microscopy study of
690 conversion of smectite to illite in mudstones of Nankai Trough: contrast with coeval
691 bentonites. *Clays and Clay Minerals*, 49(2): 109-118.
- 692 Merriman, R.J., Roberts, B., Peacor, D.R. and Hiron, S.R., 1995. Strain-Related Differences in
693 the Crystal-Growth of White Mica and Chlorite - a Tem and Xrd Study of the
694 Development of Metapelitic Microfabrics in the Southern Uplands Thrust Terrane,
695 Scotland. *Journal of Metamorphic Geology*, 13(5): 559-576.
- 696 Merriman, R.J. and Peacor, D.R., 1998. Very low-grade metapelites: mineralogy, microfabrics
697 and measuring reaction progress. In: M. Frey and D. Robinson (Editors), *Low-Grade
698 Metamorphism*. Blackwell Science.
- 699 Merriman, R.J., 2002. Contrasting clay mineral assemblages in British Lower Palaeozoic slate
700 belts: the influence of geotectonic setting. *Clay Minerals*, 37(2): 207-219.
- 701 Moore, D.M. and Reynolds, R.C.J., 1997. X-ray diffraction and the identification and analysis of
702 clay minerals. Oxford University Press, Oxford, New York.
- 703 Nadeau, P.H., Peacor, D.R., Yan, J. and Hillier, S., 2002. I-S precipitation in pore space as the
704 cause of geopressuring in Mesozoic mudstones, Egersund Basin, Norwegian Continental
705 Shelf. *American Mineralogist*, 87(11-12): 1580-1589.
- 706 Oertel, G. and Curtis, C.D., 1972. Clay-Ironstone Concretion Preserving Fabrics Due to
707 Progressive Compaction. *Geological Society of America Bulletin*, 83(9): 2597-2605.
- 708 Olszewska, B.W. and Wieczorek, J., 1998. The Palaeogene of the Podhale Basin (Polish Inner
709 Carpathians)-micropaleontological perspectives. *Przeglad Geologiczny*, 46(8/2): 721-
710 728.
- 711 Peacor, D.R., 1992. Analytical Electron-Microscopy - X-Ray-Analysis. *Reviews in Mineralogy*,
712 27: 113-140.
- 713 Perry, E. and Hower, J., 1970. Burial diagenesis in Gulf Coast pelitic sediments. *Clays and Clay
714 Minerals*, 18: 165-177.
- 715 Poprawa, P. and Marynowski, L., 2005. Thermal history of the Podhale Trough (northern part of
716 the Central Carpathian Paleogene Basin) - preliminary results from 1-D maturity
717 modeling. *Mineralogical Society of Poland - Special Papers*, 25: 352-355.
- 718 Ramseyer, K. and Boles, J.R., 1986. Mixed-Layer Illite Smectite Minerals in Tertiary Sandstones
719 and Shales, San-Joaquin Basin, California. *Clays and Clay Minerals*, 34(2): 115-124.
- 720 Rieke, H.H. and Chilingarian, G.V., 1974. Compaction of argillaceous sediments. *Compaction of
721 argillaceous sediments. Developments in Sedimentology* 16. Elsevier.
- 722 Sorby, H.C., 1853. On the origin of slaty cleavage. *Edinburgh New Philosophical Journal*, 10:
723 136.
- 724 Środoń, J., Morgan, D.J., Eslinger, E.V., Eberl, D.D. and Karlinger, M.R., 1986. Chemistry of
725 Illite Smectite and End-Member Illite. *Clays and Clay Minerals*, 34(4): 368-378.

726 Środoń, J., Clauer, N., Banas, M. and Wojtowicz, A., 2006a. K-Ar evidence for a Mesozoic
727 thermal event superimposed on burial diagenesis of the Upper Silesia Coal Basin. *Clay*
728 *Minerals*, 41(2): 669-690.

729 Środoń, J. et al., 2006b. Diagenetic history of the Podhale-Orava Basin and the underlying Tatra
730 sedimentary structural units (Western Carpathians): evidence from XRD and K-Ar of
731 illite-smectite. *Clay Minerals*, 41: 751-774.

732 Środoń, J., 2009. Quantification of illite and smectite and their layer charges in sandstones
733 and shales from shallow burial depth. *Clay Minerals*, 44: 421-434.

734 Stuart, A., Ord, J.K. and Arnold, S., 1999. *Kendall's Advanced Theory of Statistics, Volume 2A*,
735 London : Arnold ; New York : Oxford University Press.

736 Tari, G., Baldi, T. and Baldibek, M., 1993. Paleogene Retroarc Flexural Basin beneath the
737 Neogene Pannonian Basin - a Geodynamic Model. *Tectonophysics*, 226(1-4): 433-455.

738 Taylor, T.R. et al., 2010. Sandstone diagenesis and reservoir quality prediction: Models, myths,
739 and reality. *AAPG Bulletin*, 94(8): 1093-1132.

740 van de Kamp, P.C., 2008. Smectite-Illite-Muscovite transformation, Quartz Dissolution, and
741 Silica Release in Shales. *Clays and Clay Minerals*, 56(1): 66-81.

742 van der Pluijm, B.A., Lee, J.H. and Peacor, D.R., 1988. Analytical Electron-Microscopy and the
743 Problem of Potassium Diffusion. *Clays and Clay Minerals*, 36(6): 498-504.

744 Voltolini, M., Wenk, H.R., Mondol, N.H., Bjorlykke, K. and Jahren, J., 2009. Anisotropy of
745 experimentally compressed kaolinite-illite-quartz mixtures. *Geophysics*, 74(1): D13-D23.

746 Warren, E.A. and Ransom, B., 1992. The Influence of Analytical Error Upon the Interpretation
747 of Chemical Variations in Clay-Minerals. *Clay Minerals*, 27(2): 193-209.

748 Weaver, C.E., 1989. *Clays, muds, and shales. Developments in Sedimentology 44*. Elsevier,
749 Amsterdam, New York.

750 Westwalewicz-Magilska, E., 1986. Nowe spojrzenie na genezę osadów fliszu podhalanskiego.
751 *Przegląd Geologiczny*, 12: 690-698 (in Polish).

752 Yang, Y. and Aplin, A.C., 2004. Definition and practical application of mudstone porosity-
753 effective stress relationships. *Petroleum Geoscience*, 10(2): 153-162.

754 Yang, Y.L. and Aplin, A.C., 1997. A method for the disaggregation of mudstones.
755 *Sedimentology*, 44(3): 559-562.

756
757
758